Chapter 2

Radiation effect on MHD fully developed mixed convection in a vertical channel with asymmetric heating*

2.1 Introduction

Heat transfer in free and force convection in vertical channels occurs in any industrial processes and natural phenomena. Most of the interest in this subject is due to its applications, for instance, in the design of cooling systems or electronic devices, chemical processing equipment, microelectronic cooling and in the field of solar energy collections. Since some fluids can also emit and absorb thermal radiation, it is of interest to study the effects of magnetic field on the temperature distribution and heat transfer when the fluid is not only an electrical conductor but also when it is capable of emitting/absorbing radiation. Hence, heat transfer by thermal radiation is becoming of greater importance in space applications and higher operating temperatures. Ozisik [181] has mentioned in an excellent review article that heat transfer by simultaneous radiation and convection has applications in numerous technological problems, including combustion, furnace design, the design of high-temperature gas-cooled nuclear reactors, nuclear-reactor safety,

*Published in **Journal of Applied Fluid Mechanics, 7(3)(2014), pp.503-512.***

fluidized-bed heat exchangers, fire spreads, advanced energy conservation devices such as open-cycle coal and natural-gas-fired MHD, solar ponds,solar collectors, natural convection in cavities and many others. On the other hand, it is worth mentioning that heat transfer by simultaneous radiation and convection is very important in the context of space technology and processes involving high temperature. An excellent description of the fundamentals of thermal radiation has been presented in the book by Modest [182]. For a comprehensive treatment of the radiation transfer and the interactions with convection the interested reader can consult also the books by Sprrow and Cess [183], Ozisik [184], Siegel and Howell [185].

Aung [186], Aung et al. [187, 188], Aung and Worku [189], Barletta [190], Boulama and Galanis [191] have dealt with the evaluation of the temperature and velocity profiles for the vertical channel flow in fully develoved regime. As is well known, heat exchangers technology involves convective flows in vertical channels. In most cases, these flows imply conditions of uniform heating of a channel, which can be modelled either by uniform wall temperature or uniform heat flux. Radiative heat transfer becomes very important for designing the pertinent equipment in new engineering areas. Nuclear power plants, gas turbines and various propulsion devices for aircraft, missiles satellites and space vehicles are examples of such engineering areas. Cogley et al. [192] have studied the differential approximation for radiative heat transfer in a non-grey gas near equilibrium. The hydrodynamic fully developed laminar convective flow through a vertical channel in the optically thin limit has been studied by Greif et al. [193] whereas Gupta and Gupta [96] have studied the same problem in the presence of a transverse magnetic field. The effects of radiative heat transfer on MHD flows in vertical channel have been studied a number of researches. Datta and Jana [194] have discussed the effect of wall conductances on hydromagnetic convection of a radiating gas in a vertical channel. Ogulu and Motsa [195] have studied the effect of radiative heat transfer on magnetohydrodynamic Couette flow with variable wall temperature. Sharma et al. [196] have discussed the radiation effect on temperature distribution in three-dimensional Couette flow with suction/injection. The effects of wall conductance on MHD fully developed flow with asymmetric heating of the walls has been studied by Guria et al. [197]. Ghosh and Nandi [99] have discussed magnetohydrodynamic fully developed combined convection flow between verti-

cal plates heated asymmetrically. MHD fully developed mixed convection flow with asymmetric heating of the walls have been described by Ghosh et al. [100]. Pantokratoras [198] has presented his results for a steady free convection flow between vertical parallel plates by considering different conditions on the wall temperature. The thermal radiation effect on fully developed mixed convection flow in a vertical channel have been examined by Grosan and Pop [199]. Suneetha et al. [200] have investigated the thermal radiation effects on MHD flow past an impulsively started vertical plate in the presence of heat source/sink and viscous dissipation. Baoku et al. [201] have examined transient MHD Couette flow of an electrically conducting fluid in the presence of an applied transverse magnetic field and thermal radiation through a porous medium. A numerical study on unsteady hydromagnetic generalized Couette flow and heat transfer characteristics of a reactive variable viscosity electrically conducting third grade fluid in a channel in the presence of uniform transverse magnetic field has been reported by Makinde and Chinyoka [202] with asymmetric convective cooling at the walls. Rundora and Makinde [203, 204] have considered non-Newtonian fluid through a porous saturated medium with asymmetric convective heating and/or Navier slip. Gaur et al. [205] have studied transient free convective radiative flow between vertical parallel plates heated/cooled asymmetrically with heat generation and slip condition.

In the present chapter, we study the effects of radiative heat transfer on MHD fully developed mixed convective flow in a vertical channel with the asymmetric heating of walls in the presence of a transverse magnetic field. We assume that the radiative heat flux follows a relation in an optically thin limit for a non-grey gas near equilibrium. The closed form solutions for velocity, temperature, induced magnetic field, shear stresses and critical Grashof number are presented. Flow and heat transfer results for a range of values of the pertinent parameters have been reported. It is observed that the velocity field is greatly influenced by the radiative heat transfer as well as buoyancy forces. The induced magnetic field decreases near the cold wall and it increases near the hot wall of the vertical channel with an increase in radiation parameter. Further, an increase in radiation parameter leads to decrease the fluid temperature in the channel.

2.2 Formulation of the problem and its solutions

Consider a steady MHD fully developed mixed convective flow of a viscous incompressible electrically conducting fluid confined between two vertical walls. The channel walls are at a distance d apart. Choose a Cartesian co-ordinates system with x-axis in the upward direction along the cold wall in the direction of flow and y-axis is perpendicular to it(see Fig. 2.1). The wall at $y = 0$ has a uniform temperature T_2 while the wall at $y = d$ is subjected to a uniform temperature T_1, where $T_1 > T_2$. A uniform magnetic field of strength B_0 is imposed perpendicular to the walls. The flow is due to buoyancy force, difference in temperature and in the presence of pressure gradient. Since the channel walls are infinitely long along the x-direction, all physical quantities except pressure are functions of y only. The velocity components are (u, v) relative to the Cartesian frame of reference.

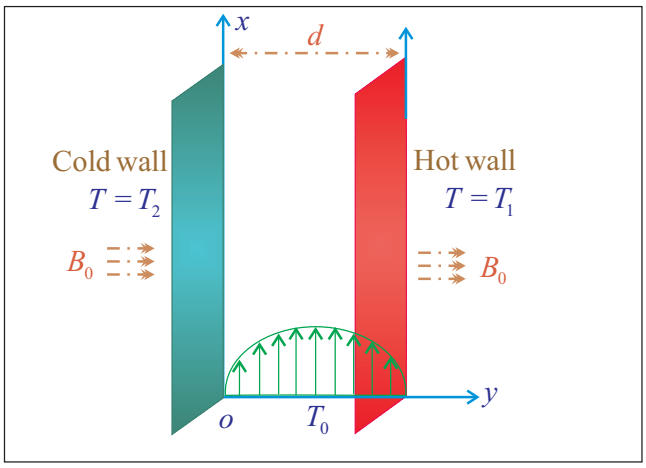

Fig.2.1: *Geometry of the problem*

The Boussinesq approximation is assumed to hold and for the evaluation of the gravitational body force, the density is assumed to depend on the temperature according to the equation of state

$$\rho = \rho_0[1 - \beta(T - T_0)], \tag{2.1}$$

where T is the fluid temperature, ρ the fluid density, β the coefficient of thermal expansion, T_0 and ρ_0 being the temperature and density at the entrance of the channel.

The solenoidal equation $\nabla.\vec{B} = 0$ gives $B_y = \text{constant} = B_0$ everywhere in the flow where $\vec{B} \equiv (B_x, B_0, 0)$. The flow being fully developed the relations $v = 0$, $\frac{\partial v}{\partial y} = 0$ and $\frac{\partial p}{\partial y} = 0$ are applied here, where p is the fluid pressure. The continuity equation gives $\frac{\partial u}{\partial x} = 0$ which in turn gives $u = u(y)$.

Using the Boussinesq approximation (2.1), the momentum and the magnetic induction equations along x-axis are

$$\mu \frac{d^2u}{dy^2} + \mu_e \, B_0 \frac{dB_x}{dy} + \rho_0 \, g \, \beta \, (T - T_0) = \frac{d\,p}{d\,x}, \tag{2.2}$$

$$\frac{d^2B_x}{dy^2} + \sigma \, \mu_e \, B_0 \frac{du}{dy} = 0, \tag{2.3}$$

and the energy equation is

$$0 = k\frac{d^2T}{dy^2} - \frac{\partial q_r}{\partial y}, \tag{2.4}$$

where μ is the coefficient of viscosity of the fluid, μ_e the magnetic permeability, σ the conductivity of the fluid, g the acceleration due to gravity, k the thermal conductivity and q_r the radiative heat flux.

It has been shown by Cogley et al. [192] that in the optically thin limit for a non-grey gas near equilibrium, the following relation holds

$$\frac{\partial q_r}{\partial y} = 4(T - T_0) \int_0^\infty K_{\lambda_0} \left(\frac{\partial e_{\lambda h}}{\partial T} \right)_0 d\lambda, \tag{2.5}$$

where K_{λ_0} is the absorption coefficient, λ is the wave length, e_{λ_h} is the Planck's function and subscript $'0'$ indicates that all quantities have been evaluated at the temperature T_0 which is the temperature at the entrance of the channel.

On the use of equation (2.5), equation (2.4) becomes

$$0 = k\frac{d^2T}{dy^2} - 4I(T - T_0), \tag{2.6}$$

where

$$I = \int_0^\infty K_{\lambda_0} \left(\frac{\partial e_{\lambda h}}{\partial T} \right)_0 d\lambda.$$

In asymmetric heating of the walls, the velocity, temperature and magnetic boundary conditions are respectively,

$$\begin{aligned} &u = 0, \;\; T = T_2 \;\text{ and }\; B_x = 0 \;\text{ at }\; y = 0, \\ &u = 0, \;\; T = T_1 \;\text{ and }\; B_x = 0 \;\text{ at }\; y = d, \end{aligned} \tag{2.7}$$

assuming the walls are electrically non-conducting.

Introducing the non-dimensional variables

$$\eta = \frac{y}{d},\ u_1 = \frac{ud}{\nu},\ b_x = \frac{B_x}{\sigma\mu_e\nu B_0},\ \ \theta = \frac{T - T_0}{T_1 - T_0} \tag{2.8}$$

equations (2.2), (2.3) and (2.6) become

$$\frac{d^2u_1}{d\eta^2} + M^2\frac{db_x}{d\eta} + Gr\ \theta + P = 0, \tag{2.9}$$

$$\frac{d^2b_x}{d\eta^2} + \frac{d\,u_1}{d\eta} = 0, \tag{2.10}$$

$$\frac{d^2\theta}{d\eta^2} - N\ \theta = 0, \tag{2.11}$$

where $M = B_0\mu_0 d\ (\sigma\ /\ \rho_0\nu)^{\frac{1}{2}}$ is the Hartmann number which may be interpreted as the ratio of induction drag to viscous drag, $Gr = \frac{g\,\beta\,(T_2 - T_1)\,d^3}{\nu^2}$ the Grashof number which signifies the relative strength of the thermal buoyancy force to the viscous force, $N = \frac{4Id^2}{k}$ the radiation parameter and $P = \frac{d^3}{\rho\nu^2}\left(-\frac{\partial p}{\partial x}\right)$ the non-dimensional pressure gradient.

The boundary conditions given by equation (2.7) also become

$$\begin{aligned} &u_1 = 0,\ \ \theta = r_T\ \text{ and }\ b_x = 0\ \text{ at }\ \eta = 0,\\ &u_1 = 0,\ \ \theta = 1\ \text{ and }\ b_x = 0\ \text{ at }\ \eta = 1, \end{aligned} \tag{2.12}$$

where $r_T = \frac{T_2 - T_0}{T_1 - T_0}$ is the temperature difference ratio.

The solution of the equations (2.9) - (2.11) subject to the boundary conditions (2.12) are

$$\theta(\eta) = \begin{cases} \frac{\sinh\sqrt{N}\,\eta}{\sinh\sqrt{N}} + r_T\frac{\sinh\sqrt{N}\,(1-\eta)}{\sinh\sqrt{N}} & N \neq M^2 \\ \\ \frac{\sinh M\,\eta}{\sinh M} + r_T\frac{\sinh M\,(1-\eta)}{\sinh M} & N = M^2, \end{cases} \tag{2.13}$$

$$u_1(\eta) = \begin{cases} \left(\frac{P}{M^2} + c\right)\left\{1 - \frac{\sinh M\,\eta}{\sinh M} - \frac{\sinh M\,(1-\eta)}{\sinh M}\right\} \\ +\frac{Gr}{N - M^2}\Big[\left\{\frac{\sinh M\,\eta}{\sinh M} + r_T\frac{\sinh M\,(1-\eta)}{\sinh M}\right\} \\ -\left\{\frac{\sinh\sqrt{N}\,\eta}{\sinh\sqrt{N}} + r_T\frac{\sinh\sqrt{N}\,(1-\eta)}{\sinh\sqrt{N}}\right\}\Big] & N \neq M^2 \\ \\ \left(\frac{P}{M^2} + c\right)\left\{1 - \frac{\sinh M\,\eta}{\sinh M} - \frac{\sinh M\,(1-\eta)}{\sinh M}\right\} \\ -\frac{Gr}{2M\sinh M}\Big[(r_T - \cosh M)\frac{\sinh M\,\eta}{\sinh M} \\ +\eta\left\{\cosh M\,\eta - r_T\cosh M\,(1-\eta)\right\}\Big] & N = M^2, \end{cases} \tag{2.14}$$

$$b_x(\eta) = \begin{cases} c_1 + c\eta - \left(\frac{P}{M^2} + c\right)\left\{\eta - \frac{\cosh M\,\eta}{M\sinh M} + \frac{\cosh M\,(1-\eta)}{M\sinh M}\right\} \\ -\frac{Gr}{N-M^2}\Big[\left\{\frac{\cosh M\,\eta}{M\sinh M} - r_T\frac{\cosh M\,(1-\eta)}{M\sinh M}\right\} \\ -\left\{\frac{\cosh\sqrt{N}\,\eta}{\sqrt{N}\sinh\sqrt{N}} - r_T\frac{\cosh\sqrt{N}\,(1-\eta)}{\sqrt{N}\sinh\sqrt{N}}\right\}\Big] & N \neq M^2 \\ \\ c_1 + c\eta - \left(\frac{P}{M^2} + c\right)\left\{\eta - \frac{\cosh M\,\eta}{M\sinh M} + \frac{\cosh M\,(1-\eta)}{M\sinh M}\right\} \\ +\frac{Gr}{2M\sinh M}\Big[(r_T - \cosh M)\frac{\cosh M\,\eta}{M\sinh M} \\ +\frac{\eta}{M}\left\{\sinh M\,\eta + r_T\sinh M\,(1-\eta)\right\} \\ -\frac{1}{M^2}\left\{\cosh M\,\eta - r_T\cosh M\,(1-\eta)\right\}\Big] & N = M^2, \end{cases} \tag{2.15}$$

$$\text{where} \quad c_1 = \begin{cases} \frac{P}{2M^2} + \frac{Gr(1-r_T)}{2(N-M^2)}\left[\frac{1+\cosh M}{M\sinh M} - \frac{1+\cosh\sqrt{N}}{\sqrt{N}\sinh\sqrt{N}}\right] & N \neq M^2 \\ \\ \frac{P}{2M^2} + \frac{Gr(1-r_T)}{4M^3\sinh^2 M}(1+\cosh M)(M+\sinh M) & N = M^2, \end{cases} \tag{2.16}$$

$$c = \begin{cases} -\frac{P}{M^2}\left\{1 + \frac{M\sinh M}{2(1-\cosh M)}\right\} + \frac{Gr(1+r_T)}{2(N-M^2)}\cdot\frac{M\sinh M}{1-\cosh M} \\ \times\left[\frac{1-\cosh M}{M\sinh M} - \frac{1-\cosh\sqrt{N}}{\sqrt{N}\sinh\sqrt{N}}\right] & N \neq M^2 \\ \\ -\frac{P}{M^2}\left\{1 + \frac{M\sinh M}{2(1-\cosh M)}\right\} + \frac{Gr(1+r_T)}{4M^2\sinh M} \\ \times(\sinh M - M) & N = M^2, \end{cases} \tag{2.17}$$

and P is given by equation (2.19). It is seen from the expressions (2.13)-(2.15) that the velocity field and induced magnetic field depend on the Grashof number Gr, whereas the temperature distribution is independent of Gr.

2.3 Expression for pressure gradient

It is noticed from the equations (2.14) and (2.15) that the parameter P is still to be evaluated. Using the rate of mass flow

$$\int_0^1 u_1\,d\eta = 1, \tag{2.18}$$

we have, on the substitution of the value of u_1, which is obtained from equation (2.14) as

$$P = \begin{cases} \frac{2M^2(\cosh M-1)}{M\sinh M+2(1-\cosh M)} + \frac{Gr(1+r_T)}{N-M^2}\cdot\frac{M^3\sinh M}{M\sinh M+2(1-\cosh M)} \\ \times\left[\frac{1-\cosh M}{M\sinh M} - \frac{1-\cosh\sqrt{N}}{\sqrt{N}\sinh\sqrt{N}}\right] & N \neq M^2 \\ \\ \frac{2M^2(\cosh M-1)}{M\sinh M+2(1-\cosh M)}\left[1 - \frac{1}{4}Gr(1+r_T)\frac{\sinh M-M}{M^2\sinh M}\right] & N = M^2. \end{cases} \tag{2.19}$$

2.4 Results and discussion

To study the effects of radiative heat transfer and magnetic field on the MHD fully developed flow with asymmetric heating of the walls, the dimensionless velocity u_1, the induced magnetic field b_x and temperature distribution θ are depicted graphically against η for several values of radiation parameter N, squared-Hartmann number M^2, buoyancy parameter Gr and temperature difference ratio r_T in Figs.2.2-2.11.

2.4.1 Velocity profiles and induced magnetic field

Figures 2.2 and 2.3 depict the effects of the radiative heat transfer and magnetic field on the velocity field. It is seen from Figure 2.2 that the fluid velocity u_1 increases in the range $0 \leq \eta \leq 0.38$ while it decreases in the range $0.38 \leq \eta \leq 0.86$ and again it increases in the range $0.86 \leq \eta \leq 1$ with an increase in radiation parameter N.

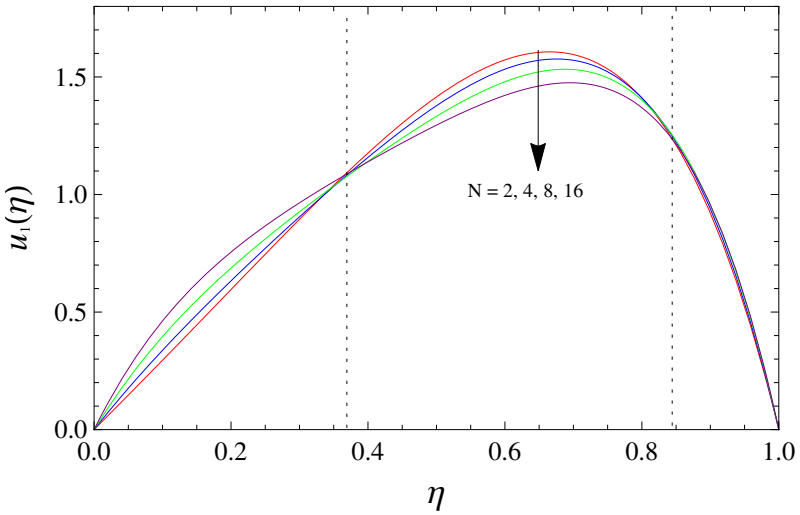

Fig.2.2: *Variation of velocity for different N when $M^2 = 5$, $r_T = 0.4$ and $Gr = 100$*

It is manifested that there is a closeness of the curves near the hot wall. Figure 2.3 reveals that the fluid velocity u_1 increases in the range $0 \leq \eta \leq 0.42$ while it decreases in the range $0.42 \leq \eta \leq 1$ with an increase in squared-Hartmann number M^2.

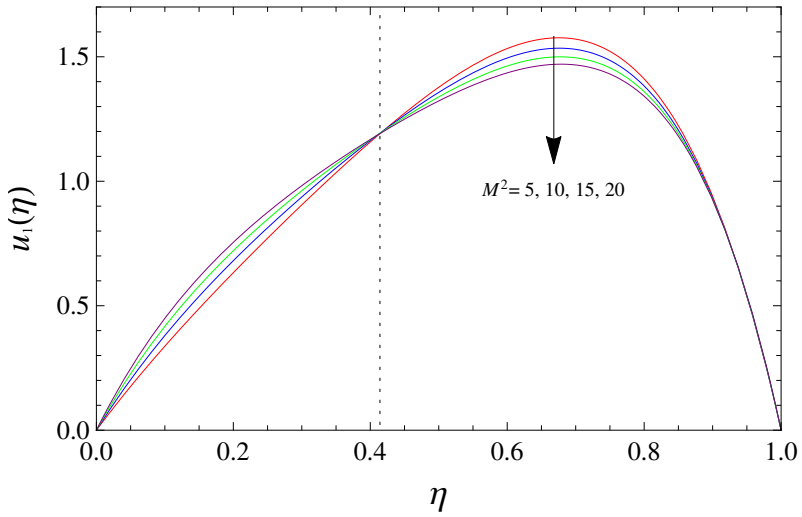

Fig.2.3: *Variation of velocity for different* M^2 *when* $N = 4$, $r_T = 0.4$ *and* $Gr = 100$

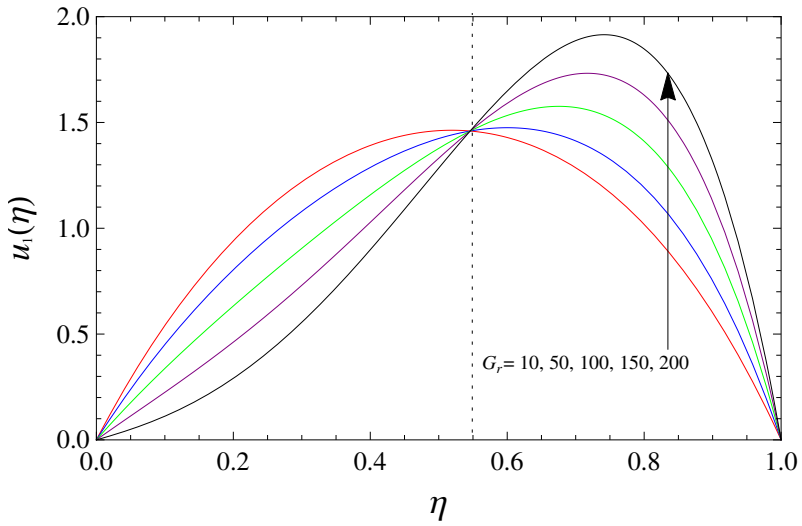

Fig.2.4: *Variation of velocity for different* Gr *when* $M^2 = 5$, $N = 4$ *and* $r_T = 0.4$

It means that the Lorentz force imposed by a transverse magnetic field to an electrically conducting fluid, which slows down the fluid motion near the hot wall and enhances the fluid motion near the cold wall. It is also manifested that there is a closeness of the curves near the hot wall. Figure 2.4 shows that the fluid velocity u_1 decreases in the region $0 \leq \eta \leq 0.53$ and it increases in the region $0.53 \leq \eta \leq 1$ with an increase in Grashof number Gr.

Figure 2.5 shows that with an increase in r_T, the fluid velocity u_1 increases in the region $0 \leq \eta \leq 0.47$ and it decreases in the region $0.47 \leq \eta \leq 1$.

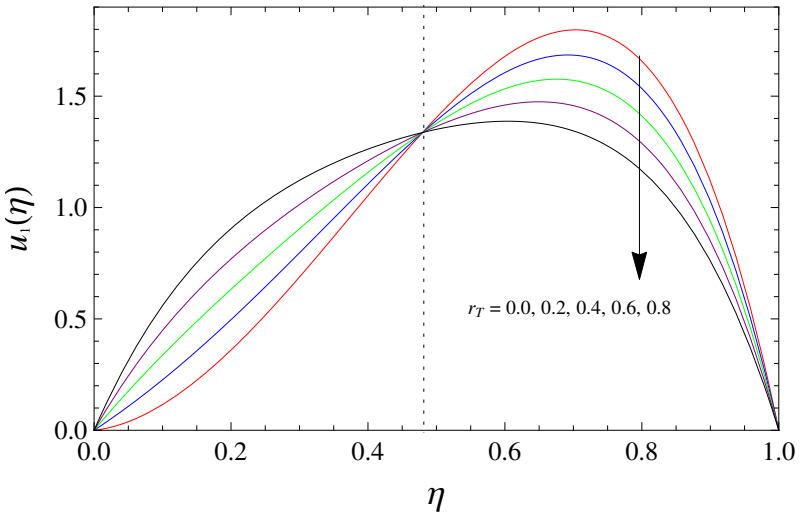

Fig.2.5: *Variation of velocity for different r_T when $M^2 = 5$, $N = 4$ and $Gr = 100$*

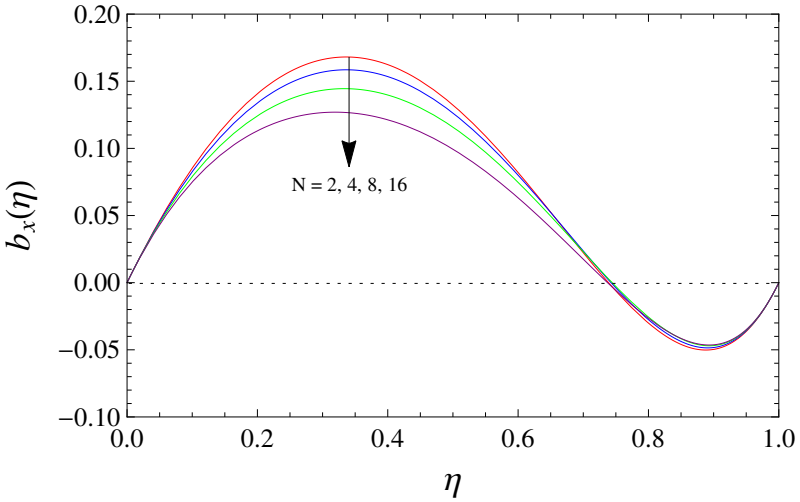

Fig.2.6: *Variation of induced magnetic field for different N when $M^2 = 5$, $r_T = 0.4$ and $Gr = 100$*

It is observed from Figure 2.6 that the induced magnetic field b_x decreases at any point near the cold wall and it increases near the hot wall with an increase in radiation parameter N. Figure 2.7 shows that the induced magnetic field b_x decreases with an increase in M^2.

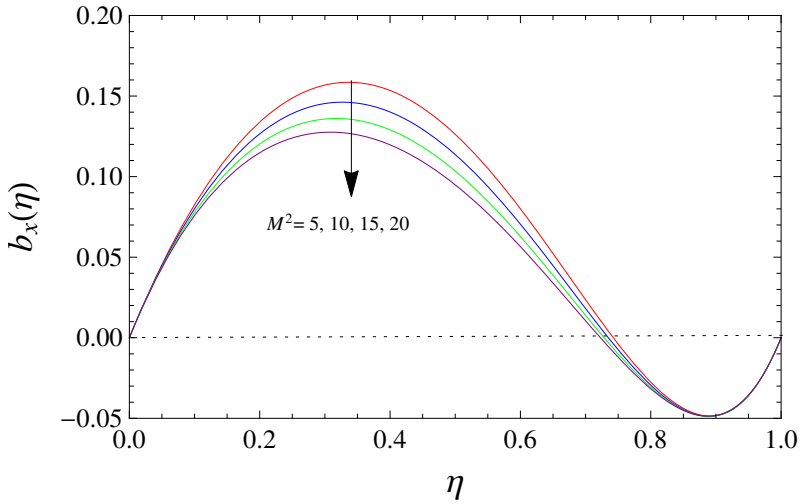

Fig.2.7: *Variation of induced magnetic field for different* M^2 *when* $N = 4$, $r_T = 0.4$ *and* $Gr = 100$

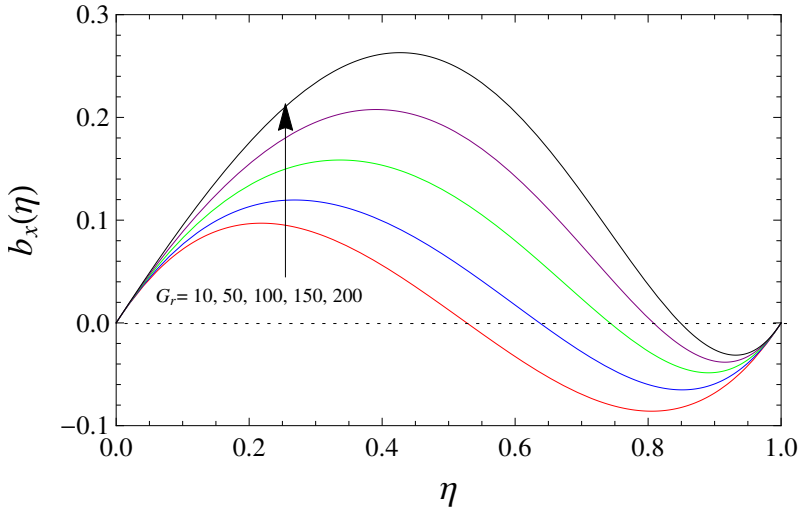

Fig.2.8: *Variation of induced magnetic field for different* Gr *when* $N = 4$, $r_T = 0.4$ *and* $M^2 = 5$

It is seen from Figure 2.8 that the induced magnetic field b_x increases with an increase in Gr. Figure 2.9 reveals that the induced magnetic field b_x decreases with an increase in r_T.

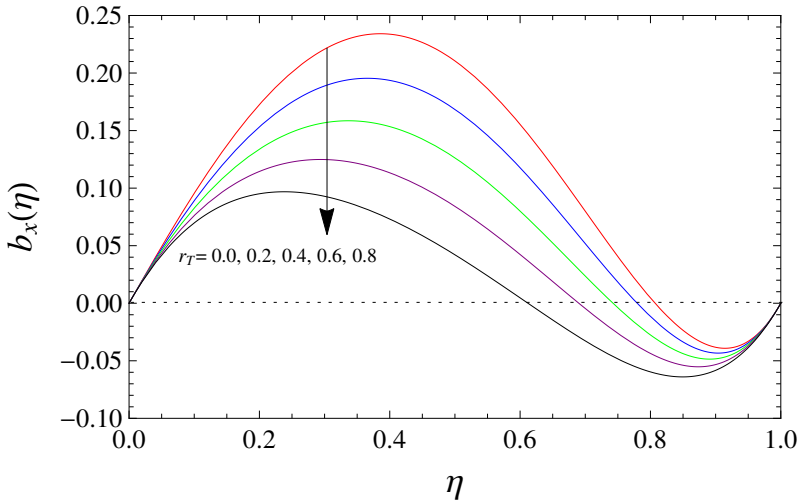

Fig.2.9: *Variation of induced magnetic field for different* r_T *when* $N = 4$, $M^2 = 5$ *and* $Gr = 100$

2.4.2 Temperature profile

The temperature profiles have been drawn for different values of N and r_T in Figures 2.10 and 2.11. It is seen from Figures 2.10 and 2.11 that the fluid temperature θ decreases with an increase in radiation parameter N while it increases with an increase in temperature difference ratio parameter r_T.

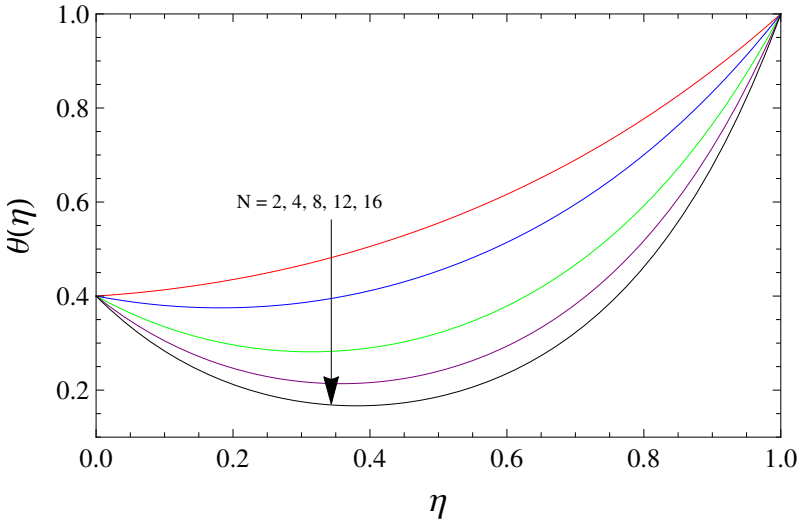

Fig.2.10: *Variation of temperature for different* N *when* $r_T = 0.4$

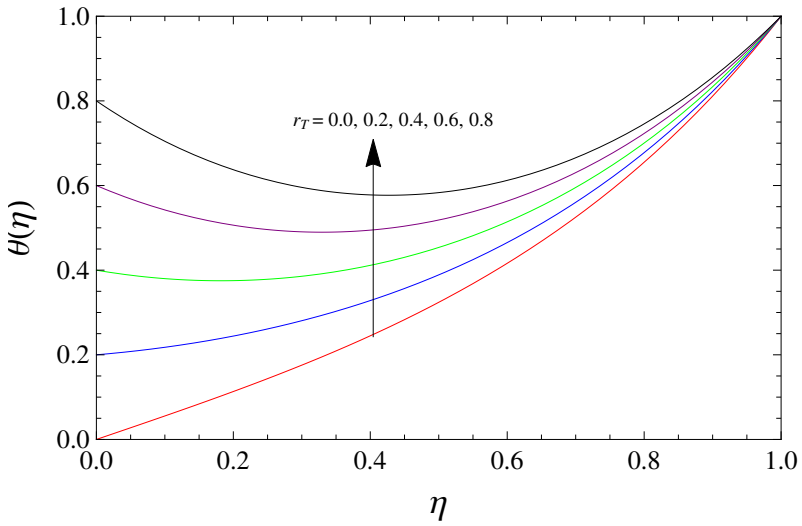

Fig.2.11: *Variation of temperature for different r_T when $N = 4$*

2.4.3 Shear stresses

One of the important characteristics of this problem is the shear stress at the walls. The non-dimensional shear stresses at the cold wall ($\eta = 0$) and hot wall ($\eta = 1$) are respectively given by

$$\tau_{x_0} = \left(\frac{du_1}{d\eta}\right)_{\eta=0} \quad \text{and} \quad \tau_{x_1} = \left(\frac{du_1}{d\eta}\right)_{\eta=1}, \tag{2.20}$$

where

$$\tau_{x_0} = \begin{cases} \frac{M^2(\cosh M-1)}{M\sinh M+2(1-\cosh M)}\left[1+\frac{Gr(1+r_T)}{N-M^2}\left(\frac{1-\cosh M}{M\sinh M}-\frac{1-\cosh\sqrt{N}}{\sqrt{N}\sinh\sqrt{N}}\right)\right] \\ +\frac{Gr}{N-M^2}\left[\frac{M(1-r_T\cosh M)}{\sinh M}-\frac{\sqrt{N}(1-r_T\cosh\sqrt{N})}{\sinh\sqrt{N}}\right] \qquad N\neq M^2 \\ \frac{M^2(\cosh M-1)}{M\sinh M+2(1-\cosh M)}\left[1+Gr(1+r_T)\frac{(1-\cosh M)(\sinh M-M)}{2M^3\sinh^2 M}\right] \\ -\frac{Gr}{2M\sinh M}\left[(r_T-\cosh M)\frac{M}{\sinh M}+(1-r_T\cosh M)\right] \quad N=M^2, \end{cases} \tag{2.21}$$

and

$$\tau_{x_1} = \begin{cases} \frac{M^2(1-\cosh M)}{M\sinh M+2(1-\cosh M)}\left[1+\frac{Gr(1+r_T)}{N-M^2}\left(\frac{1-\cosh M}{M\sinh M}-\frac{1-\cosh\sqrt{N}}{\sqrt{N}\sinh\sqrt{N}}\right)\right] \\ +\frac{Gr}{N-M^2}\left[\frac{M(\cosh M-r_T)}{\sinh M}-\frac{\sqrt{N}(\cosh\sqrt{N}-r_T)}{\sinh\sqrt{N}}\right] \qquad N\neq M^2 \\ \frac{M^2(1-\cosh M)}{M\sinh M+2(1-\cosh M)}\left[1+Gr(1+r_T)\frac{(1-\cosh M)(\sinh M-M)}{2M^3\sinh^2 M}\right] \\ -\frac{Gr}{2M\sinh M}\left[(r_T\cosh M-1)\frac{M}{\sinh M}+(\cosh M-r_T)\right] \quad N=M^2. \end{cases} \tag{2.22}$$

The values of non-dimensional shear stresses at the walls ($\eta = 0$) and ($\eta = 1$) are shown graphically against r_T for different values of N and M^2 in Figures 2.12 and 2.13. It is observed from Figure 2.12 that for fixed values of M^2 and Gr, the shear stress τ_{x_0} at the cold wall and the magnitude of the shear stress τ_{x_1} at the hot wall increase with an increase in radiation parameter N. Figure 2.13 shows that the shear stress τ_{x_0} at the cold wall and the magnitude of the shear stress τ_{x_1} at the right wall increase with an increase in M^2. It is interesting to note that the shear stress due to the flow does not vanish at the walls ($\eta = 0$) and ($\eta = 1$) when buoyancy forces $Gr = 0$. Thus we arrive an interesting conclusion that there is no flow reversal in the absence of the buoyancy forces.

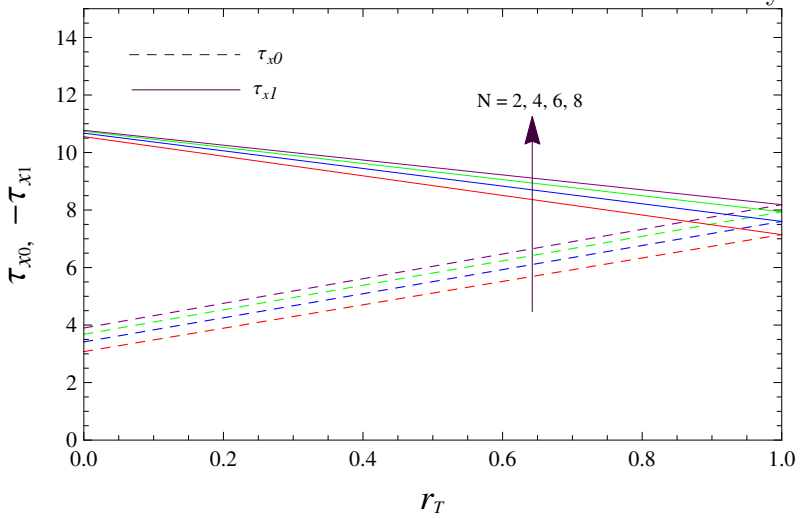

Fig.2.12: *Shear stresses for different N when $M^2 = 5$ and $Gr = 50$*

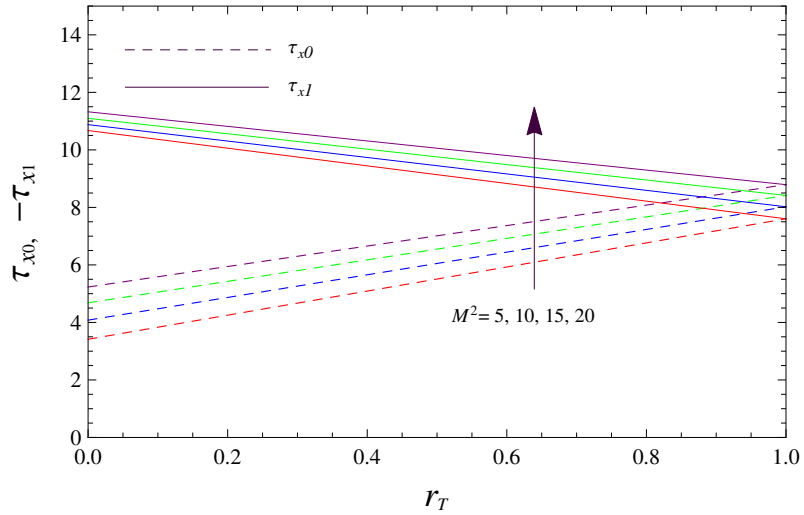

Fig.2.13: *Shear stresses for different M^2 when $N = 4$ and $Gr = 50$*

The shear stresses at the cold and hot wall vanish if

$$Gr_0 = \begin{cases} \frac{(N-M^2)M^2(1-\cosh M)}{(A+B)[M\sinh M+2(1-\cosh M)]} & N \neq M^2 \\ \\ \frac{2M^2(1-\cosh M)}{(A+B)[M\sinh M+2(1-\cosh M)]} & N = M^2, \end{cases} \tag{2.23}$$

$$Gr_1 = \begin{cases} \frac{(N-M^2)M^2(1-\cosh M)}{(A_1+B_1)[M\sinh M+2(1-\cosh M)]} & N \neq M^2 \\ \\ \frac{2M^2(1-\cosh M)}{(A_1+B_1)[M\sinh M+2(1-\cosh M)]} & N = M^2, \end{cases} \tag{2.24}$$

where

$$A = \begin{cases} \frac{M^2(1+r_T)(\cosh M-1)}{M\sinh M+2(1-\cosh M)}\left[\frac{1-\cosh M}{M\sinh M}-\frac{1-\cosh\sqrt{N}}{\sqrt{N}\sinh\sqrt{N}}\right] & N \neq M^2 \\ \\ \frac{(1+r_T)(1-\cosh M)^2(M-\sinh M)}{M\sinh^2 M[M\sinh M+2(1-\cosh M)]} & N = M^2, \end{cases} \tag{2.25}$$

$$B = \begin{cases} \frac{M(1-r_T\cosh M)}{\sinh M}-\frac{\sqrt{N}(1-r_T\cosh\sqrt{N})}{\sinh\sqrt{N}} & N \neq M^2 \\ \\ \frac{M(\cosh M-r_T)+\sinh M(r_T\cosh M-1)}{M\sinh^2 M} & N = M^2, \end{cases} \tag{2.26}$$

$$A_1 = \begin{cases} \frac{M^2(1+r_T)(1-\cosh M)}{M\sinh M+2(1-\cosh M)}\left[\frac{1-\cosh M}{M\sinh M}-\frac{1-\cosh\sqrt{N}}{\sqrt{N}\sinh\sqrt{N}}\right] & N \neq M^2 \\ \\ \frac{(1+r_T)(1-\cosh M)^2(\sinh M-M)}{M\sinh^2 M[M\sinh M+2(1-\cosh M)]} & N = M^2, \end{cases} \tag{2.27}$$

$$B_1 = \begin{cases} \frac{M(\cosh M-r_T)}{\sinh M}-\frac{\sqrt{N}(\cosh\sqrt{N}-r_T)}{\sinh\sqrt{N}} & N \neq M^2 \\ \\ \frac{M(1-r_T\cosh M)+\sinh M(r_T-\cosh M)}{M\sinh^2 M} & N = M^2. \end{cases} \tag{2.28}$$

The values of the critical Grashof numbers Gr_0 and Gr_1 due to the flow at the cold wall ($\eta = 0$) and hot wall ($\eta = 1$) are entered in the Tables-2.1 and 2.2 for different values of squared-Hartmann number M^2, radiation parameter N and the temperature difference ratio parameter r_T. It is seen from the Table-2.1 that the critical Grashof number Gr_0 at the cold wall ($\eta = 0$) due to the flow increases with an increase in either N or r_T or M^2. Table-2.2 shows that the critical Grashof number Gr_1 at the hot wall ($\eta = 1$) due to the flow increases with an increase in either M^2 or r_T. On the other hand, with an increase in the radiation parameter N, the critical Grashof number Gr_1 decreases.

Table-2.1: *The values of critical Grashof number* $Gr_0 \times 10^{-3}$ *at the cold wall*

M^2	N			r_T		
	2.0	4.0	6.0	0.00	0.20	0.40
5	0.1821947	0.2327067	0.2946396	0.1056287	0.1453024	0.2327067
10	0.2102455	0.2710896	0.347127	0.1214226	0.1677217	0.2710896
15	0.2385835	0.3102064	0.4012581	0.1373196	0.1903684	0.3102064
20	0.2671151	0.3498836	0.4567396	0.1532741	0.2131661	0.3498836

Table-2.2: *The values of critical Grashof number* $Gr_1 \times 10^{-3}$ *at the hot wall*

M^2	N			r_T		
	2.0	4.0	6.0	0.00	0.20	0.40
5	0.1197925	0.109435	0.1033845	0.07737131	0.09065144	0.109435
10	0.1361429	0.123871	0.1167035	0.08797246	0.10288010	0.123871
15	0.1524667	0.138243	0.1299393	0.09855560	0.11507350	0.138243
20	0.1687417	0.152538	0.1430853	0.10910590	0.1272174	0.1525389

In the absence of radiative heat transfer ($N = 0$), the critical Grashof numbers Gr_0 and Gr_1 are given by

$$Gr_0 = \frac{2M^4(\cosh M - 1)}{(1 - r_T)[M^2(1 + \cosh M) + 4\cosh M - 4(1 + \cosh M)]}, \quad (2.29)$$

$$Gr_1 = -Gr_0, \quad (2.30)$$

which are identical with equation (39) of Guria et al. [197].

2.4.4 Limiting case

Now, we shall discuss the case when the radiation parameter $N \ll 1$. In this case, equations (2.13)-(2.15) become

$$\theta(\eta) = \eta + \frac{N}{6}(\eta^3 - \eta) + r_T\left[(1 - \eta) + \frac{N}{6}\eta(1 - \eta)(\eta - 2)\right], \quad (2.31)$$

$$u_1(\eta) = \left(\frac{P}{M^2} + c\right)\left\{1 - \frac{\sinh M\,\eta}{\sinh M} - \frac{\sinh M\,(1 - \eta)}{\sinh M}\right\}$$

$$+ \quad \frac{Gr}{(N-M^2)}\Bigg[\left\{\frac{\sinh M\,\eta}{\sinh M}+r_T\frac{\sinh M\,(1-\eta)}{\sinh M}\right\}$$
$$- \quad \left[\eta+\frac{N}{6}(\eta^3-\eta)+r_T\left\{(1-\eta)+\frac{N}{6}\eta(1-\eta)(\eta-2)\right\}\right]\Bigg], \quad (2.32)$$

$$b_x(\eta) = \frac{P}{2M^2}+\frac{Gr(1-r_T)}{2(N-M^2)}\cdot\frac{1+\cosh M}{M\sinh M}+c\eta$$
$$- \left(\frac{P}{M^2}+c\right)\left\{\eta-\frac{\cosh M\,\eta}{M\sinh M}+\frac{\cosh M\,(1-\eta)}{M\sinh M}\right\}$$
$$- \frac{Gr}{(N-M^2)}\left\{\frac{\cosh M\,\eta}{M\sinh M}-r_T\frac{\cosh M\,(1-\eta)}{M\sinh M}\right\}$$
$$- \frac{3Gr}{(N-M^2)(N+6)}\left\{\frac{1}{2}(1-r_T)-\eta^2+r_T(1-2\eta+\eta^2)\right\}, \quad (2.33)$$

where

$$c = \left[-\frac{P}{M^2}+\frac{Gr(1+r_T)}{2(N-M^2)}\right]\left[\frac{M\sinh M+2(1-\cosh M)}{2(\cosh M-1)}\right],$$
$$P = \frac{2M^2(\cosh M-1)}{M\sinh M+2(1-\cosh M)}+\frac{M^2Gr(1+r_T)}{2(N-M^2)}. \quad (2.34)$$

In the limit $N \to 0$, equations (2.31)-(2.33) for the temperature, velocity and induced magnetic filed yield respectively

$$\theta(\eta) = \eta+r_T(1-\eta), \quad (2.35)$$
$$u_1(\eta) = \frac{1}{M^2}\left[\left(Gr\,r_T+P+M^2\,c\right)\left\{1-\frac{\sinh M\eta}{\sinh M}-\frac{\sinh M(1-\eta)}{\sinh M}\right\}\right.$$
$$+ \left. Gr(1-r_T)\left(\eta-\frac{\sinh M\eta}{\sinh M}\right)\right], \quad (2.36)$$

$$b_x(\eta) = -\frac{1}{M^2}\left[(Gr\,r_T+P+M^2c)\left\{\eta-\frac{\cosh M\eta}{M\sinh M}+\frac{\cosh M(1-\eta)}{M\sinh M}\right\}\right.$$
$$+ \left. Gr\,(1-r_T)\left(\frac{1}{2}\,\eta^2-\frac{\cosh\,M\eta}{M\sinh\,M}\right)\right]+c\eta+c_1, \quad (2.37)$$

where

$$c = \left[Gr\;r_T+P+\frac{1}{2}Gr(1-r_T)\right]\left[\frac{M\sinh M+2(1-\cosh M)}{2M^2(\cosh M-1)}\right],$$
$$c_1 = \frac{1}{2M^2}\Bigg[(Gr\;r_T+P)$$

$$+ \quad \frac{1}{2}Gr(1-r_T)\left\{\frac{M\sinh M - 2(1+\cosh M)}{M\sinh M}\right\}\Bigg], \tag{2.38}$$

$$P = \frac{2M^2(\cosh M - 1)}{M\sinh M + 2(1-\cosh M)} - \frac{1}{2}Gr(1+r_T).$$

The velocity and the induced magnetic field given by equations (2.36) and (2.37) coincide with the equations (14) and (15) of Guria et al. [197] in the case of without wall conductance.

2.5 Conclusion

An analytical study has been presented to expose the impact of radiative heat transfer on MHD mixed convective flow in a vertical channel with asymmetric heating of the walls. The Cogley heat flux model is considered in the energy equation and the temperature of the walls are assumed to be constant. The closed form solutions of momentum, magnetic induction and energy equations are obtained analytically in usual manner. A limiting consideration of radiation has been taken to validate the results. The impressive results are listed below:

- The squared-Hartmann number slows down the fluid motion near the hot wall and enhances near the cold wall.
- As radiation parameter increases, the induced magnetic field decreases near the cold wall while it increases near the hot wall of the channel.
- With increasing radiation parameter, the fluid temperature is lowering within the channel.
- The shear stress at the cold wall increases while that at the hot wall decreases with increasing radiation parameter.
- In the absence of the buoyancy force, there is no flow reversal in the channel.
- The critical Grashof numbers at both the channel walls increase with an increase in either squared-Hartmann number M^2 or temperature difference ratio r_T.
- Radiation causes to increase the critical Grashof number near the cold wall while it causes to decrease near the hot wall.